Available online at www.sciencedirect.com
ScienceDirect
European Journal of Mechanics B/Fluids 28 (2009) 61–71

Vortex formation in lid-driven arc-shape cavity flows at high Reynolds numbers

Hatice Mercan, Kunt Atalık *

Mechanical Engineering Department, Boğaziçi University, 34342 Bebek, Istanbul, Turkey

Received 2 August 2007; received in revised form 17 January 2008; accepted 19 February 2008

Available online 23 February 2008

Abstract

High-Reynolds number lid-driven flow in arc-shape cavities with different cross sections is considered up to $Re = 8000$. The unsteady streamfunction–vorticity transport formulation is adopted and a second order finite difference numerical method is applied to computational grids generated by body-fitted coordinate transformation. The effects of aspect or arc angle ratio r, on the formation and growth of vortical structures, as well as on the existence and development of periodic solutions are discussed. It is found that for the case where $r > 1/2$, only a secondary vortex appears in addition to a primary core vortex, for stationary solutions, whereas tertiary and quaternary vortices appear for the cases where $r < 1/2$, near the curved wall. Periodic solutions at high Reynolds numbers are observed when $r \geqslant 1/2$; while transient oscillations decay in time for $r < 1/2$.

Keywords: Lid-driven flow; Arc-shape cavity; Vortex formation; High Reynolds number

1. Introduction

The flow problem in lid-driven cavities has been a popular research subject due to its wide range of physical applications for which the structure of inertia induced vortices in a cavity needs to be investigated in detail. The lid-driven cavity problem has also been used as a classical benchmark case to test new numerical schemes and methods [1–3]. Most of the studies in the literature are concerned with the square or rectangular cavity flows, although in applications, the cavities may be non-rectangular. There are few studies dealing with flows in curved cavities driven by a moving lid. Tillmark [4] carried out an experimental and numerical study on the lid-driven flow in a polar cavity. In a series of papers, Cheng et al. [5–7] studied experimentally and numerically the effects of buoyancy and convective heat transfer on the flow pattern inside an arc-shape cavity. Migeon et al. [8] studied experimentally the effects of lid-driven cavity shape on the flow establishment phase for square, rectangular and semi-circular cavities. Recently, Glowinski et al. [9] applied a finite element method to the wall-driven flow in a semi-circular cavity and revealed the vortex structure at high Reynolds numbers. They also identified a Hopf bifurcation leading to periodicity of solutions around a Reynolds number of $Re = 6600$.

* Corresponding author. Tel.: +90 212 359 4573; fax: +90 212 287 2456.
E-mail address: atalik@boun.edu.tr (K. Atalık).

0997-7546/$ – see front matter
doi:10.1016/j.euromechflu.2008.02.001

In the present work, we aim to study the formation and establishment of vortical structures at high Reynolds numbers up to $Re = 8000$, in arc-shape cavities of different cross sections, including the semi-circular cavity as a test case. We also aim to observe periodicity of solutions in transient and steady-state flow regimes, and to identify the effect of cross sectional shape determined by the aspect ratio or arc angle ratio r, on the existence of periodic solutions, reported in [9] for a semi-circular cavity. The unsteady streamfunction-vorticity transport formulation is adopted. Body fitted coordinate transformation is applied to generate an elliptic computational grid. The governing equations are discretized in space using second-order finite differences. The streamfunction equation is solved using the iterative method of successive over relaxation with Chebyshev acceleration. Coupled to it, the vorticity transport equation is solved in time using a second-order explicit Adams–Bashforth scheme. The primary, secondary and higher vortical structures formation and establishment are compared for different arc-shape cavity cross sections. The existence of periodic solutions in transient and steady-state flow regimes is investigated.

2. Formulation and numerical solution method

We consider an arc-shape cavity of height H and with a lid of length L at the top, moving at a constant speed U_0 to the right. Different cross sectional cavities are considered, which correspond to different aspect ratios H/L. They are also characterized by the ratio, r, of the arc angle to 2π. Five different cross sections are considered, corresponding to $r = 2/3$, $r = 1/2$, $r = 1/3$, $r = 1/4$ and $r = 1/5$ ratios. The arc angle ratio $r = 1/2$ corresponds to semi-circular case.

It is possible to transform the physical domain of the cavity to a rectangular computational domain in two dimensions. The transformation gives rise to a body fitted coordinate system [10,11], in which the coordinate lines are given by the images of uniform coordinate lines in the computational domain. We then consider the mapping from the computational domain (ξ, η) to physical domain (x, y). The elliptic grid generation equations are given as,

$$\alpha x_{\xi\xi} - 2\beta x_{\xi\eta} + \gamma x_{\eta\eta} = 0, \tag{1}$$

$$\alpha y_{\xi\xi} - 2\beta y_{\xi\eta} + \gamma y_{\eta\eta} = 0 \tag{2}$$

where the subscripts denote partial differentiation and α, β, γ are transformation metrics which are written as,

$$\alpha = x_\eta^2 + y_\eta^2, \tag{3}$$

$$\beta = x_\xi x_\eta + y_\xi y_\eta, \tag{4}$$

$$\gamma = x_\xi^2 + y_\xi^2. \tag{5}$$

The grid orthogonality is controlled by vanishing second transformation metric β. In this work, for the grids that have been generated by the elliptic grid generation technique, the order of magnitude of the second transformation metric β is 10^{-6}. An example of a generated elliptic grid is given in Fig. 1.

To model the flow inside the cavity, we use streamfunction-vorticity transport formulation. Choosing the lid length L as a length scale, and the lid speed U_0 as a velocity scale, the non-dimensional flow equations in curvilinear coordinates are,

$$\alpha\psi_{\xi\xi} - 2\beta\psi_{\xi\eta} + \gamma\psi_{\eta\eta} = -J^2\omega, \tag{6}$$

$$\omega_t + \frac{1}{J}\left[(y_\eta u\omega_\xi - y_\xi u\omega_\eta) + (x_\xi v\omega_\eta - x_\eta v\omega_\xi)\right] = \frac{1}{Re\,J^2}(\alpha\omega_{\xi\xi} - 2\beta\omega_{\xi\eta} + \gamma\omega_{\eta\eta}) \tag{7}$$

where ψ represents the streamfunction, ω is the vorticity, u and v are the velocity components in (x, y) plane and J is the Jacobian of the transformation which is written as,

$$J = x_\xi y_\eta - x_\eta y_\xi. \tag{8}$$

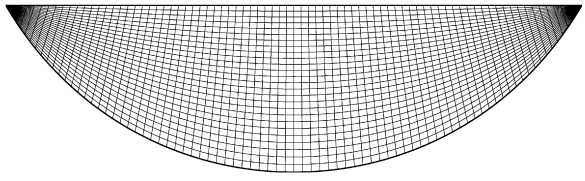

Fig. 1. (27×81) grid sample for $r = 1/3$ arc cavity.

The non-dimensional Reynolds number is defined with respect to fluid density ρ and viscosity μ as $Re = \rho U_0 L/\mu$. The time variable is non-dimensionalized by choosing the time scale as L/U_0. In this work, L and U_0 are set to be equal to unity. The boundary conditions are no-slip conditions.

The equations are discretized using a second order centered difference scheme in space and an explicit second-order Adams–Bashforth scheme in time. The discretized streamfunction equation (6) is solved coupled to the vorticity transport equation (7), by using the iterative method of successive over relaxation with Chebyshev acceleration to accelerate the rate of convergence [12].

The boundary conditions, on stationary walls are written as,

$$u = 0, \quad v = 0, \quad \psi = 0, \quad \omega_w = \left[\frac{3}{\Delta h^2}(\psi_w - \psi_{w-1}) + \frac{\omega_{w-1}}{2} \right] \tag{9}$$

and on the moving lid they become,

$$u = U_0, \quad v = 0, \quad \psi = 0, \quad \omega_w = \left[\frac{3}{\Delta h^2}(\psi_w - \psi_{w-1}) + \frac{\omega_{w-1}}{2} + \frac{3U_0}{\Delta h} \right]. \tag{10}$$

The above discretized form of the vorticity boundary condition follows Woods formula [13], and takes into account interior values of vorticity as well. The subscript w denotes the value at the boundary whereas $w-1$ denotes the neighboring value in the direction normal to the surface. Δh is the space difference between the two adjacent points calculated for the grid with appropriate metrics.

3. Numerical tests and comparisons

Convergence tests for different Reynolds numbers have been performed on 61×61, 81×81 and 101×101 grids, for $r = 1/3$ and $r = 1/4$ arc cavity cases at $Re = 5000$ and $Re = 6500$. The difference for minimum and maximum streamfunction values was of the order of 10^{-4} between 81×81 and 101×101 grids. Finally, a 101×101 grid is chosen to be used in the simulation results presented in this work. Numerical result comparisons with previous works are given in Tables 1 and 2. The minimum and maximum streamfunction values are shown for $r = 1/3$ ratio arc geometry in Table 1 at $Re = 100$, $Re = 1000$ and $Re = 1500$. The corresponding values are shown for $r = 1/2$ ratio arc geometry (semi-circular case) in Table 2 at $Re = 5000$ and $Re = 6600$. The streamlines are shown for $r = 1/3$ ratio case at $Re = 1000$ in Fig. 2(a), and at $Re = 1500$, in Fig. 2(b). For $r = 1/2$ semi-circular case, the streamlines at $Re = 5000$ and at $Re = 6600$ are given in Fig. 2(c) and in Fig. 2(d), respectively. They agree with the results in [5] and [9].

Numerical simulations by Glowinski et al. [9] show a secondary vortex beginning to form at $t \simeq 6$. Their non-dimensional time definition is the same as the definition used in this paper. Migeon et al. [8] carried out experiments

Table 1
The minimum and maximum streamfunction values for $r = 1/3$ arc cavity

Re		$\psi_{\min}$	$\psi_{\max}$
100	[5]	−0.0415832	0.0
	[Present]	−0.0416261	0.0
1000	[5]	−0.0450499	0.0001003
	[Present]	−0.0452365	0.0000918
1500	[5]	−0.0437994	0.0016739
	[Present]	−0.0441206	0.0016934

Table 2
The minimum and maximum streamfunction values for $r = 1/2$ arc cavity

Re		$\psi_{\min}$	Location	$\psi_{\max}$	Location
5000	[9]	−0.0726	(0.6809, −0.1988)		
	[Present]	−0.0694	(0.7132, −0.1825)	0.01236	(0.2676, −0.2137)
6600	[9]	−0.0673	(0.7006, −0.1894)		
	[Present]	−0.0656	(0.7464, −0.1704)	0.01581	(0.3020, −0.2208)

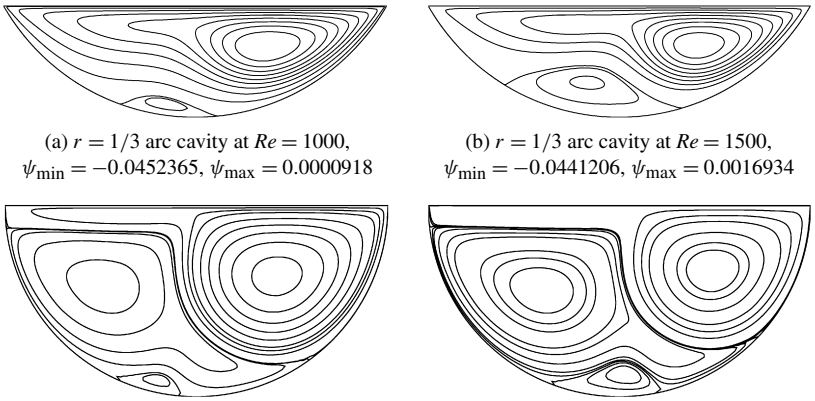

(a) $r = 1/3$ arc cavity at $Re = 1000$, $\psi_{\min} = -0.0452365$, $\psi_{\max} = 0.0000918$

(b) $r = 1/3$ arc cavity at $Re = 1500$, $\psi_{\min} = -0.0441206$, $\psi_{\max} = 0.0016934$

(c) $r = 1/2$ arc cavity at $Re = 5000$, $\psi_{\min} = -0.0694$, $\psi_{\max} = 0.01236$

(d) $r = 1/2$ arc cavity at $Re = 6600$, $\psi_{\min} = -0.0656$, $\psi_{\max} = 0.01581$

Fig. 2. Streamlines at different Reynolds numbers for $r = 1/3$ and $r = 1/2$ arc cavities.

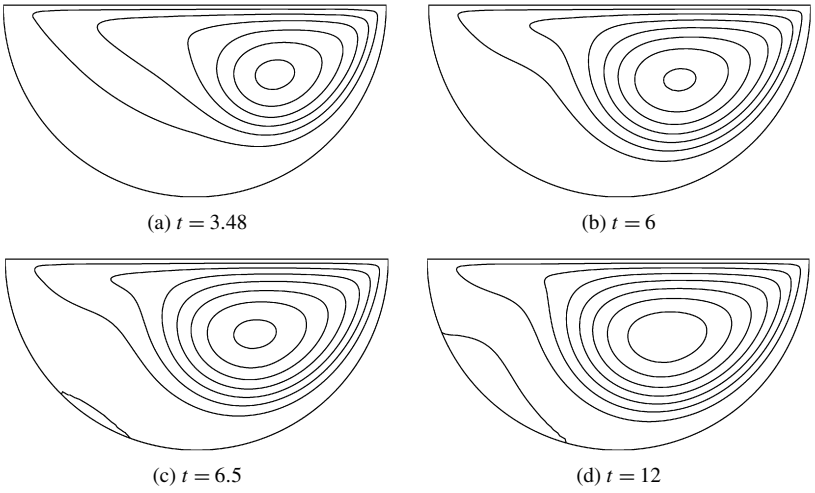

(a) $t = 3.48$

(b) $t = 6$

(c) $t = 6.5$

(d) $t = 12$

Fig. 3. Time evolution of streamlines for $r = 1/2$ arc cavity at Reynolds number $Re = 1000$.

to study the flow establishment in a semi-circular cavity, and reported a homogeneous and uniform recirculation or primary vortex with no secondary flow, at $Re = 1000$, for a final time of observation corresponding to our non-dimensional time (defined above) $t \simeq 3.5$, as also noted in [9]. The flow establishment test results are shown in Figs. 3(a)–3(d). Our results agree with both the experimental observations and previous numerical simulations, with no secondary vortex up to $t \simeq 6$, and with a secondary vortex appearing at $t \simeq 6.5$ and growing to reach a steady state size at $t \simeq 12$.

4. Results and discussion

4.1. Vortex structure

For the considered arc angle ratios, the steady state vortical structures for different Reynolds numbers are observed and compared. It is accepted that the steady state is reached according to a relative difference norm E of the vorticity at each $(k+1)$th Adams–Bashforth time step with respect to the previous kth time step as

$$E = \sqrt{\frac{\sum_{i,j=1}^{N_\xi, N_\eta} (\omega^{k+1}(i,j) - \omega^{k}(i,j))^2}{\sum_{i,j=1}^{N_\xi, N_\eta} (\omega^{k+1}(i,j))^2}} \tag{11}$$

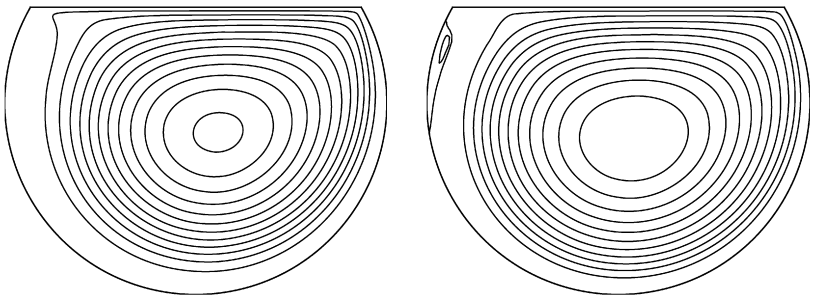

(a) $Re = 1000$, $\psi_{\min} = -0.122557$, $\psi_{\max} = 0.0$

(b) $Re = 3000$, $\psi_{\min} = -0.120525$, $\psi_{\max} = 0.00006883$

(c) $Re = 5000$, $\psi_{\min} = -0.115461$, $\psi_{\max} = 0.00063078$

(d) $Re = 7000$, $\psi_{\min} = -0.122939$, $\psi_{\max} = 0.00291456$

Fig. 4. Streamlines at different Reynolds numbers for $r = 2/3$ arc cavity case.

where N_ξ and N_η denote the number of grid points in the ξ and η directions respectively. In the simulations for presented steady state results this E value is of the order of 10^{-8} and below.

For all the cases, the primary core vortex forming at small Reynolds numbers, is shifted in the direction of the lid motion as the Reynolds number is increased. For $r = 2/3$, a secondary vortex forms near the upper left corner when the Reynolds number approaches $Re = 3000$ (Figs. 4(a)–4(b)). This secondary vortex grows with increasing Reynolds number as it can be seen (Figs. 4(c)–4(d)). The corresponding vorticity lines can be observed in Figs. 5(a)–5(d).

For $r = 1/2$ semi-circular case, the vortex structure is as given in the numerical tests at Figs. 2(c)–2(d) and comparisons at Table 3 of the previous section. In accordance with the results in [9], a secondary vortex forms near the lower left part of curved wall when Reynolds number is around $Re = 1000$ (Fig. 3(d)), and grows with increasing Reynolds number up to $Re = 7000$ to cover almost the entire left half part of the cavity. A tertiary vortex appears at the left bottom part at $Re = 5000$ and grows with increasing Reynolds number [9].

For $r = 1/3$, as the Reynolds number is increased beyond $Re = 1500$, the secondary vortex which formed at the lower left curved wall region at $Re = 1000$ (Fig. 2(a)), grows in the direction of lid motion and occupies the entire bottom of the curved wall (Fig. 6(a)), while the primary vortex is subdivided in two vortices, one occupying the upper central region, the other located at the upper right corner. When the Reynolds number is further increased, the upper central vortex grows and occupies the central region while the bottom vortex splits up in two vortices, one in the left and the other in the right lower curved wall regions (Fig. 6(b)). The splitting up of the bottom vortex occurs when the Reynolds number is between $4000 < Re < 4250$. Their sizes become approximately equal when $Re = 8000$ (Fig. 6(d)). The corresponding vorticity lines can be observed in Figs. 7(a)–7(d).

For $r = 1/4$, a secondary vortex forms at the bottom of the curved wall at $Re = 1500$ (Fig. 8(a)). This vortex grows in size and covers a larger portion of the bottom, while the core vortex shifting to the right corner is subdivided into two vortices, one in the central region, the other in the upper right corner (Figs. 8(b)–8(e)). At $Re = 4750$, the secondary vortex at the bottom part of the curved wall is observed to be divided into two vortices, one in the left and the other in the right bottom part of the curved wall (Fig. 8(c)). The splitting up of the bottom vortex occurs when the Reynolds number is between $4500 < Re < 4750$. If the Reynolds number is further increased, the left bottom vortex grows, while the right bottom vortex becomes smaller in size (Fig. 8(e)).

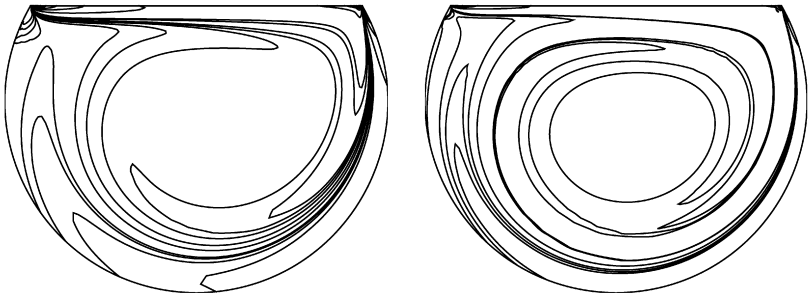

(a) $Re = 1000$ (b) $Re = 3000$

(c) $Re = 5000$ (d) $Re = 7000$

Fig. 5. Vorticity lines at different Reynolds numbers for $r = 2/3$ arc cavity case.

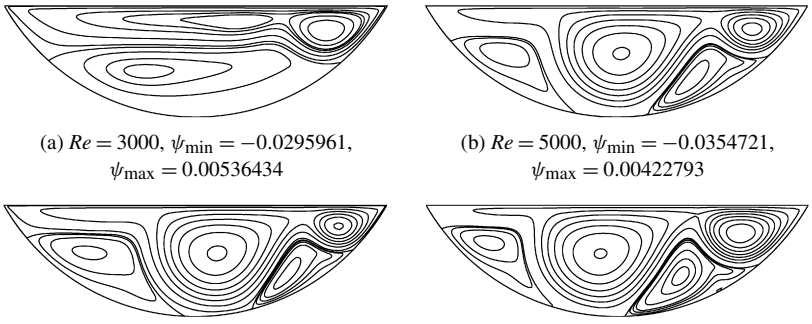

(a) $Re = 3000$, $\psi_{\min} = -0.0295961$, $\psi_{\max} = 0.00536434$

(b) $Re = 5000$, $\psi_{\min} = -0.0354721$, $\psi_{\max} = 0.00422793$

(c) $Re = 6000$, $\psi_{\min} = -0.0356826$, $\psi_{\max} = 0.00402288$

(d) $Re = 8000$, $\psi_{\min} = -0.0389991$, $\psi_{\max} = 0.00645591$

Fig. 6. Streamlines at different Reynolds numbers for $r = 1/3$ arc cavity case.

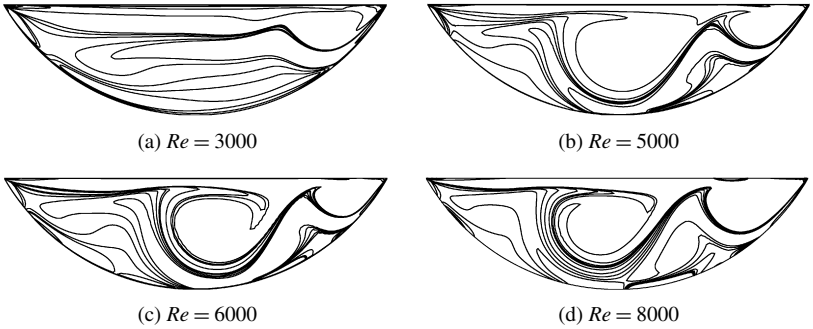

(a) $Re = 3000$ (b) $Re = 5000$

(c) $Re = 6000$ (d) $Re = 8000$

Fig. 7. Vorticity lines at different Reynolds numbers for $r = 1/3$ arc cavity case.

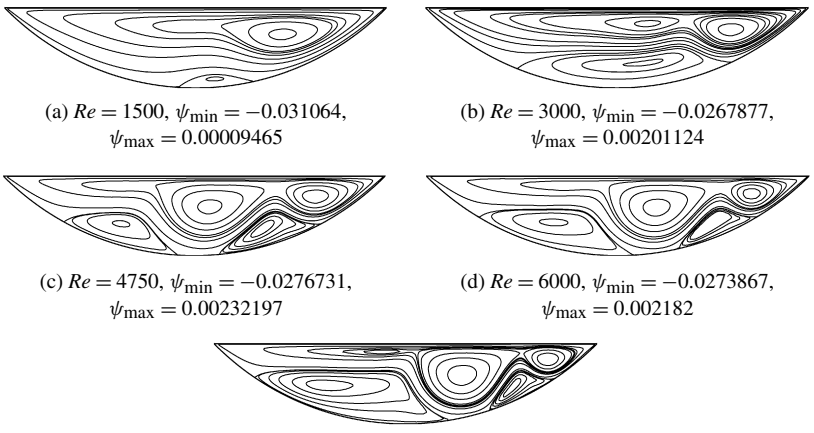

(a) $Re = 1500$, $\psi_{\min} = -0.031064$, $\psi_{\max} = 0.00009465$

(b) $Re = 3000$, $\psi_{\min} = -0.0267877$, $\psi_{\max} = 0.00201124$

(c) $Re = 4750$, $\psi_{\min} = -0.0276731$, $\psi_{\max} = 0.00232197$

(d) $Re = 6000$, $\psi_{\min} = -0.0273867$, $\psi_{\max} = 0.002182$

(e) $Re = 8000$, $\psi_{\min} = -0.0272293$, $\psi_{\max} = 0.0022504$

Fig. 8. Streamlines at different Reynolds numbers for $r = 1/4$ arc cavity case.

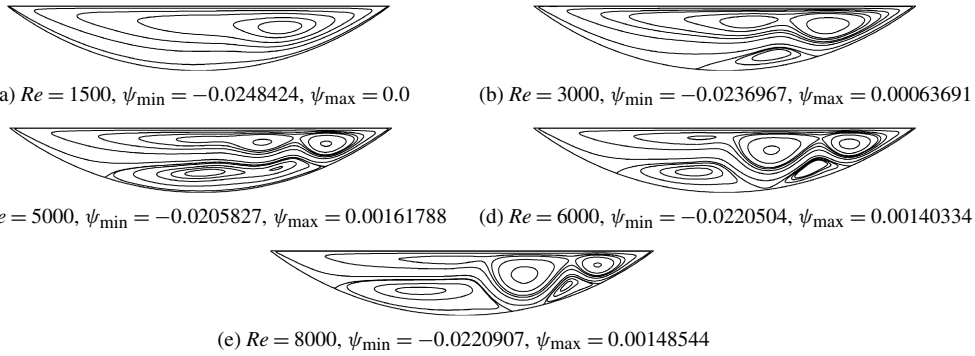

(a) $Re = 1500$, $\psi_{\min} = -0.0248424$, $\psi_{\max} = 0.0$

(b) $Re = 3000$, $\psi_{\min} = -0.0236967$, $\psi_{\max} = 0.00063691$

(c) $Re = 5000$, $\psi_{\min} = -0.0205827$, $\psi_{\max} = 0.00161788$

(d) $Re = 6000$, $\psi_{\min} = -0.0220504$, $\psi_{\max} = 0.00140334$

(e) $Re = 8000$, $\psi_{\min} = -0.0220907$, $\psi_{\max} = 0.00148544$

Fig. 9. Streamlines at different Reynolds numbers for $r = 1/5$ arc cavity case.

Finally for $r = 1/5$, the secondary vortex at the bottom part forms at a higher Reynolds number (near $Re = 3000$), compared to previous cases (Figs. 9(a)–9(b)). At $Re = 3000$, we also observe that the core vortex is subdivided into two vortices (Fig. 9(b)). At $Re = 5000$, this secondary vortex begins to split up in two vortices, one in the left and the other in the right bottom regions (Figs. 9(c)–9(d)). The splitting up of the bottom vortex occurs when $Re > 5000$. As in the case of $r = 1/4$, when the Reynolds number is further increased, the left bottom vortex grows, while the right bottom vortex becomes smaller in size (Fig. 9(e)). Compared to previous $r = 1/4$ case, the size ratio of left bottom vortex to right bottom vortex is greater.

4.2. Periodicity of solutions

In [9], a Hopf bifurcation has been reported for semi-circular lid driven cavity problem, at a Reynolds number around $Re = 6600$. Our results for the same cavity indicate this Hopf bifurcation leading to periodicity of solutions at a Reynolds number $Re = 6650$ in accordance with the results in [9] (Fig. 10). The speed evolution and its phase portrait at a point near the upper left corner can be observed in this figure for $Re = 6650$. Long time integrations indicate oscillations of amplitude of the order of 10^{-2} and with a period $\tau \simeq 1.15$. For other arc angle ratios, we investigate the periodicity of transient and steady state solutions up to Reynolds number $Re = 8000$. For the case $r = 2/3$, a Hopf bifurcation is found around $Re \simeq 7500$ and oscillatory solutions are settled at long times. Time evolution of speed at a point near the center and its phase portrait can be observed in Fig. 11, with oscillations of amplitude of the order of 10^{-3} and a period $\tau \simeq 2.69$. The periodic pattern of streamlines is given in Fig. 12, for an nth period where n is an integer. The vortex near the left part of the curved wall is observed to split up in two smaller vortices which in turn merge in one again in each period. For Reynolds numbers less than $Re \simeq 7500$, no such periodicity has been noticed.

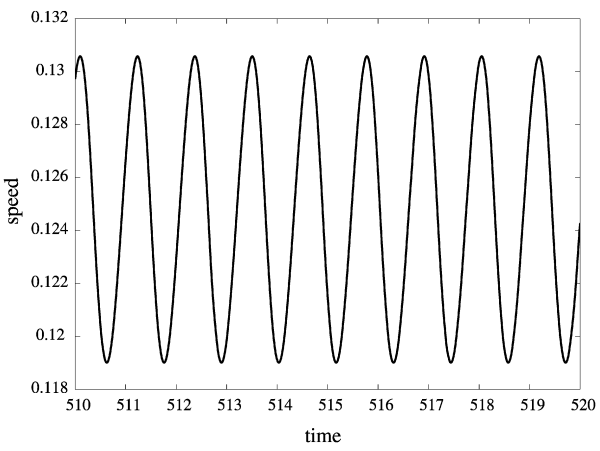

(a) Time evolution

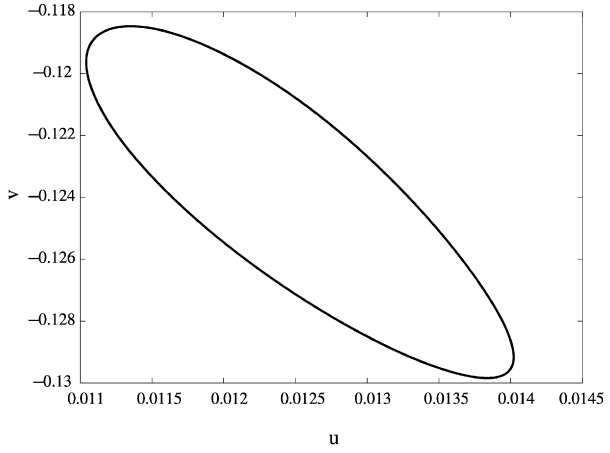

(b) Phase portrait

Fig. 10. Time evolution of speed and its phase portrait at point (0.0385, −0.1290) near the upper left corner for $r = 1/2$ arc cavity at $Re = 6650$.

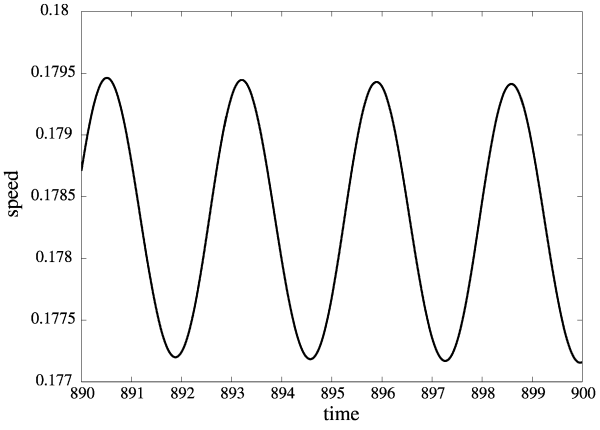

(a) Time evolution

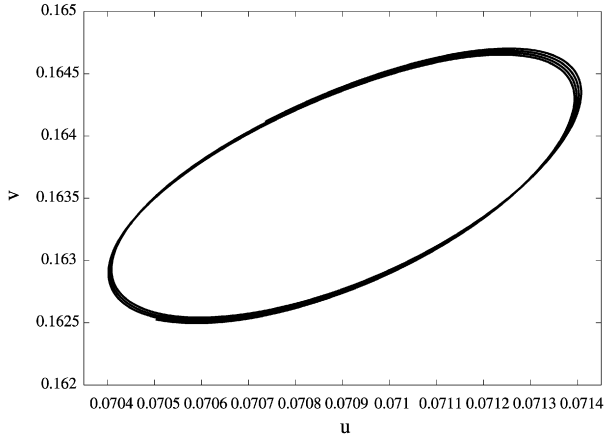

(b) Phase portrait

Fig. 11. Time evolution of speed and its phase portrait at point (0.3529, −0.3423) near the center for $r = 2/3$ arc cavity at $Re = 7500$.

For the cases $r = 1/3$, $r = 1/4$ and $r = 1/5$, time evolution of speed at a point near the upper left corner is given in Fig. 13 up to non-dimensional time $t = 100$, for $Re = 8000$. Although we observe some oscillations at early times, no steady state periodic solutions exist for these cases. However, a slowly decaying periodic solution can be observed for the case $r = 1/4$. Near $t \simeq 100$, the oscillations are of the magnitude of the order of 10^{-3}.

4.3. Flow establishment

It is first noted that for $r \geqslant 1/2$, although the vortical structures settle at early time, periodicity settles at large time (at $t \simeq 350$ for $r = 1/2$ at $Re = 6650$ and at $t \simeq 800$ for $r = 2/3$ at $Re = 7500$). For $r < 1/2$, no steady-state periodic solutions exist, however, considering the rich vortex structure, we focus on the cases $r = 1/3$, $r = 1/4$ and $r = 1/5$, to observe the time formation of recirculating zones. We present the case of $r = 1/5$ at $Re = 6000$ in Fig. 14. First the right corner vortex is formed together with a lower right vortex at $t \simeq 1$. Then a central vortex forms and grows. The lower right vortex grows to reach a final size at $t \simeq 3$, while a second vortex near the moving lid forms at $t \simeq 1.5$ and grows up to $t \simeq 3$. A small vortex at the bottom forms at $t \simeq 3$ and grows to reach a steady size at $t \simeq 15$. The flow structures are observed to settle at $t \simeq 20$.

The flow establishment for $r = 1/4$ arc cavity is similar at high Reynolds numbers. However for $r = 1/3$ arc cavity, although the vortical structures have similarities to $r = 1/4$ and $r = 1/5$ arc cavity cases, there are differences in flow establishment. In Fig. 15, it can be observed that the lower vortex forming at curved wall at $t \simeq 1$, grows considerably

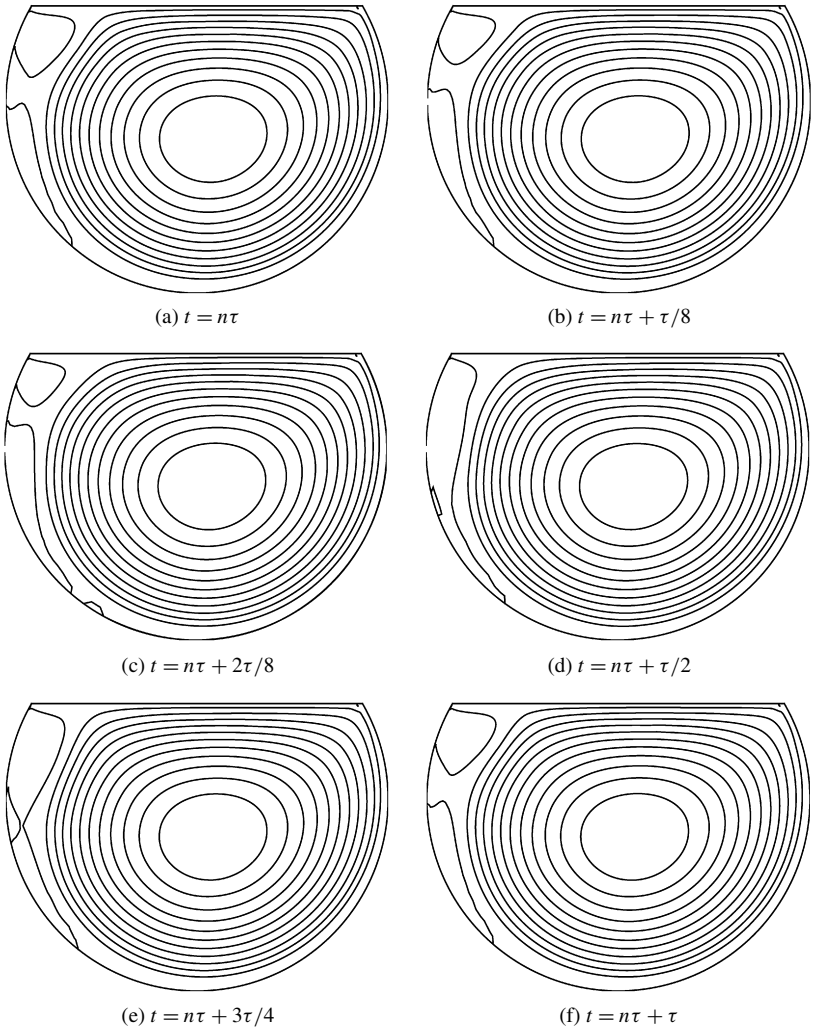

(a) $t = n\tau$ (b) $t = n\tau + \tau/8$

(c) $t = n\tau + 2\tau/8$ (d) $t = n\tau + \tau/2$

(e) $t = n\tau + 3\tau/4$ (f) $t = n\tau + \tau$

Fig. 12. Streamlines pattern in one period for $r = 2/3$ arc cavity case at Reynolds number $Re = 7500$.

Table 3
Summary of the effect of aspect ratio on the formation of vortices and periodicity

r	H/L	Secondary vortex	Tertiary vortex	Quaternary vortex	Periodicity of the solution
2/3	0.8660	$Re \approx 3000$			$Re \approx 7500$
1/2	0.5	$Re \approx 1000$	$Re \approx 5000$		$Re \approx 6650$
1/3	0.2887	$Re \approx 1000$	$Re \approx 2000$	$Re \approx 4250$	
1/4	0.2071	$Re \approx 1500$	$Re \approx 2500$	$Re \approx 4750$	
1/5	0.1625	$Re \approx 3000$	$Re \approx 3000$	$Re \approx 5000$	

up to $t \simeq 5$ to cover all lower right and central parts. This vortex then splits up into a lower left and lower right vortices up to $t \simeq 15$. The flow structures settle at $t \simeq 30$.

5. Concluding remarks

In summary, aspect ratio or arc angle ratio has a considerable effect on the flow establishment and vortical structures as well as on the nature of steady state solutions in arc shape cavities, at high Reynolds numbers. The main results are summarized in Table 3.

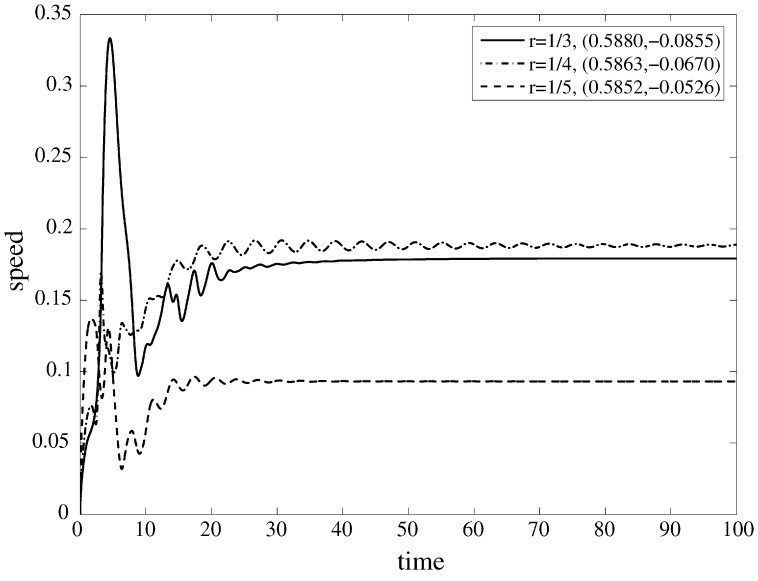

Fig. 13. Time evolution of speed at a point near the upper left corner for $r = 1/3$, $r = 1/4$, $r = 1/5$ arc cavities at Reynolds number $Re = 8000$.

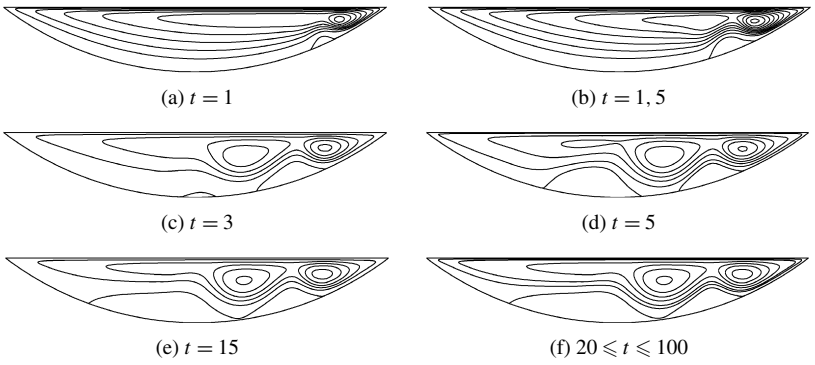

(a) $t = 1$ (b) $t = 1, 5$

(c) $t = 3$ (d) $t = 5$

(e) $t = 15$ (f) $20 \leqslant t \leqslant 100$

Fig. 14. Time evolution of streamlines for $r = 1/5$ arc cavity case at Reynolds number $Re = 6000$.

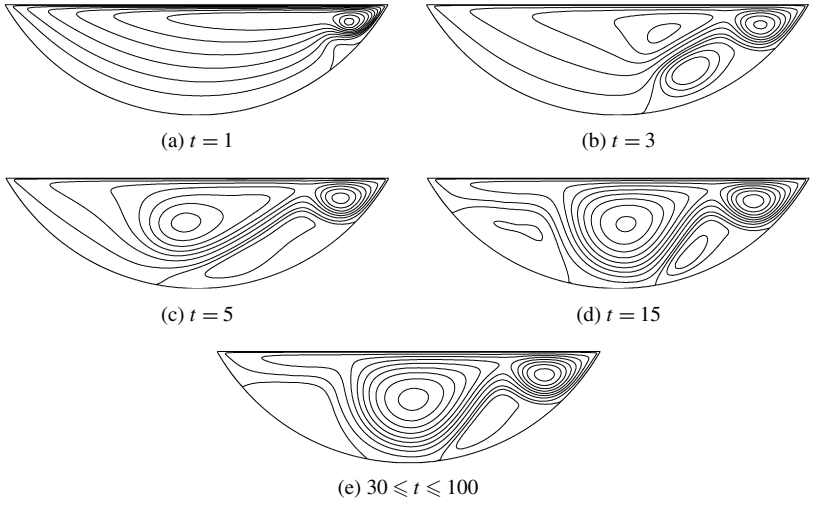

(a) $t = 1$ (b) $t = 3$

(c) $t = 5$ (d) $t = 15$

(e) $30 \leqslant t \leqslant 100$

Fig. 15. Time evolution of streamlines for $r = 1/3$ arc cavity case at Reynolds number $Re = 5000$.

For $r = 2/3$ arc cavity, only a secondary vortex near the upper left corner in addition to the primary core vortex appears and grows with increasing Reynolds number, for stationary solutions.

For $r = 1/2$ arc cavity, the vortex structure consists of the secondary vortex which grows in size and covers the left part of the cavity with increasing Reynolds number, as well as a tertiary vortex which appears at the bottom of the cavity (curved wall) as observed also in [9].

For $r = 1/3$, $r = 1/4$ and $r = 1/5$ arc cavity cases, the final vortex structures at high Reynolds numbers are much richer and a quaternary vortex appears from the splitting up of the secondary bottom vortex, in addition to upper right corner and central vortices. However, the relative sizes of left and right bottom vortices depend on the arc angle. Their sizes are almost equal for $r = 1/3$ at high Reynolds number. The left bottom vortex becomes greater in size compared to right bottom vortex for $r = 1/4$ and even greater for $r = 1/5$.

It is noted that the secondary vortex is formed at higher Reynolds numbers as r is decreased from $r = 1/3$ to $r = 1/5$. Also, the splitting up of the bottom vortex into a left and right vortex, occurs at higher Reynolds numbers as r is decreased from $r = 1/3$ to $r = 1/5$.

Periodic solutions have been observed for $r = 1/2$ arc cavity, at $Re = 6650$, similar to results reported in [9]. Such periodic solutions are also found for $r = 2/3$ arc cavity case, at $Re = 7500$ for long times. The period of oscillations is noted to be larger compared to $r = 1/2$ case. However for $r = 1/3$, $r = 1/4$ and $r = 1/5$, transient periodic solutions are observed to decay at advanced time, for Reynolds numbers up to $Re = 8000$. In the case of $r = 1/4$, the periodic nature of the transient solutions is more pronounced and the decay of periodicity is observed to be much slower compared to $r = 1/3$ and $r = 1/5$ cases.

Acknowledgements

This work is supported by Boğaziçi University Research Fund with project code 05HA602.

References

[1] O. Botella, R. Peyret, Benchmark spectral results on the lid-driven cavity flow, Comput. & Fluids 27 (1998) 421–433.
[2] C.H. Bruneau, C. Jouron, An efficient scheme for solving steady incompressible Navier–Stokes equations, J. Comput. Phys. 89 (1990) 389–413.
[3] E. Barragy, G.F. Carey, Stream function–vorticity driven cavity solutions using p finite elements, Comput. & Fluids 26 (1997) 453–468.
[4] L. Fuchs, L.N. Tillmark, Numerical and experimental study of driven flow in a polar cavity, Int. J. Numer. Methods Fluids 5 (1985) 311–329.
[5] M.H. Chang, C.H. Cheng, Prediction of lid-driven flow and heat convection in an arc-shape cavity, Int. Comm. Heat Mass Transfer 26 (6) (1999) 829–838.
[6] C.L. Chen, C.H. Cheng, Experimental and numerical study of mixed convection and flow pattern in a lid-driven arc-shape cavity, Heat Mass Transfer 41 (2004) 58–66.
[7] C.H. Cheng, C.L. Chen, Buoyancy-induced periodic flow and heat transfer in lid-driven cavities with different cross-sectional shapes, Int. Comm. Heat Mass Transfer 32 (2005) 483–490.
[8] C. Migeon, A. Texier, G. Pineau, Effects of lid driven cavity shape on the flow establishment phase, J. Fluids Struct. 14 (2000) 469–488.
[9] R. Glowinski, G. Guidoboni, T.W. Pan, Wall driven incompressible viscous flow in a two-dimensional semi-circular cavity, J. Comput. Phys. 216 (2006) 76–91.
[10] J.F. Thompson, F.C. Thames, C.W. Mastin, Automatic numerical generation of body-fitted curvilinear coordinate system for field containing any number of arbitrary two-dimensional bodies, J. Comput. Phys. 15 (1974) 299–319.
[11] F.C. Thames, J.F. Thompson, C.W. Mastin, R.L. Walker, Numerical solution for viscous and potential flow about arbitrary two-dimensional bodies using body-fitted coordinate system, J. Comput. Phys. 24 (1977) 245–273.
[12] W.H. Press, S.A. Teukolsky, W.T. Vetterling, B.P. Flannery, Numerical Recipes in FORTRAN: The Art of Scientific Computing, Cambridge University Press, Cambridge, 1992.
[13] E. Weinan, J.G.F. Liu, Vorticity boundary condition and related issues for finite difference schemes, J. Comput. Phys. 124 (1996) 364–382.